Evidence for a vascular contribution to diffusion FMRI at high *b* value

Karla L. Miller[†‡], Daniel P. Bulte[†], Hannah Devlin[†], Matthew D. Robson[§], Richard G. Wise[¶], Mark W. Woolrich[†], Peter Jezzard[†], and Timothy E. J. Behrens[†‖]

[†]Centre for Functional MRI of the Brain (FMRIB), [§]Oxford Centre for Clinical Magnetic Resonance (OCMR), and [‖]Department of Experimental Psychology, University of Oxford, Oxford, Oxon OX3 9DU, United Kingdom; and [¶]Cardiff University Brain Research Imaging Centre (CUBRIC), Cardiff University, Cardiff CF10 3AT, United Kingdom

Edited by Marcus E. Raichle, Washington University School of Medicine, St. Louis, MO, and approved November 8, 2007 (received for review August 2, 2007)

Recent work has suggested that diffusion-weighted functional magnetic resonance imaging (FMRI) with strong diffusion weighting (high *b* value) detects neuronal swelling that is directly related to neuronal firing. This would constitute a much more direct measure of brain activity than current methods and represent a major advance in neuroimaging. However, it has not been firmly established that the observed signal changes do not reflect residual vascular effects, which are known to exist at low *b* value. This study measures the vascular component of diffusion FMRI directly by using hypercapnia, which induces blood flow changes in the absence of a change in neuronal firing. Hypercapnia elicits a similar diffusion FMRI response to a visual stimulus including a rise in percent signal change with increasing *b* value, which was reported for visual activation. Analysis of the response timing found no evidence for an early response at high *b* value, which has been reported as evidence for a nonhemodynamic response. These results suggest that a large component of the diffusion FMRI signal at high *b* value is vascular rather than neuronal.

brain activation | diffusion MRI | functional MRI | neuronal swelling

Functional neuroimaging has enabled major advances in the study of normal and pathological brain function. However, the methods that provide the greatest coverage and spatial resolution, including positron emission tomography (1, 2) and magnetic resonance imaging (MRI) (3, 4), are indirect measures of neuronal activity based on metabolically driven changes in blood flow. These hemodynamic measures suffer from spatial and temporal confounds (5, 6), are nonlinearly related to neuronal firing (7, 8), and depend on baseline hemodynamics that are uncoupled from the activity of interest (9, 10). An imaging method that detects neuronal activity more directly while achieving whole-brain coverage would therefore represent a significant advance for neuroscience.

One alternative method is diffusion-weighted functional MRI (DFMRI), which attenuates the MRI signal in a manner that depends on the amount of motion (diffusion and flow) in the underlying tissue. In general, this attenuation is described by a factor $exp(-bD)$, where D is the apparent diffusion coefficient of the local tissue, and b is an acquisition parameter that describes the strength of diffusion contrast. At low b value, true diffusive motion is more difficult to detect, and the "apparent diffusion" is dominated by local blood flow (11–14). In general, diffusion weighting is directional, so that attenuation depends on the diffusion and flow parameters along the applied direction. Different signal sources have been proposed in DFMRI depending on the b value. Early work used low b value, which is thought to reflect tissue perfusion (11–16). Recent work suggested that DFMRI at high b value detects cellular swelling that is a direct consequence of neural firing (17, 18), which would constitute a more direct measure of neuronal activity.

A recent study at high b value DFMRI (18) described two findings that were considered to support the cellular-swelling hypothesis. First, the percent signal change rose with increasing b value, which is the opposite behavior to that described at low b value (14, 19, 20). Second, the response at high b value preceded the conventional FMRI response by several seconds. It was argued that these results indicated that the signal at high b value represents a true diffusion effect rather than a vascular effect with significant onset delay (18). However, the DFMRI is also intrinsically sensitive to the blood oxygenation level-dependent (BOLD) effect used in conventional FMRI, and residual vascular effects represent an important confound, even at high b value.

The cell-swelling hypothesis leads to the crucial prediction that a vascular response in the absence of a change in neural activity will not elicit a rise in signal change with increasing b value. In this study, we induce mild hypercapnia, which modulates the BOLD signal (10, 21) with negligible change to the underlying neuronal firing (22–24) or oxygen metabolism (25–27). This enables direct measurement of the vascular component of the DFMRI signal, providing a mechanism for distinguishing the contributions of neuronal activity and hemodynamics. If DFMRI does not exhibit signal changes due to hypercapnia where a change should be statistically detectable, that provides evidence that the signal responds directly to neuronal firing; alternatively, if we observe similar behavior of the DFMRI signal during hypercapnia as with a neuronal stimulus, that provides evidence for a vascular contribution.

Results

Three separate experiments were conducted to investigate the vascular contribution to DFMRI. The first two experiments replicate the acquisition paradigm from ref. 18 under visual (Experiment 1) and hypercapnic (Experiment 2) stimuli in a cohort of seven subjects. These data enable us to investigate the vascular contribution to high b value DFMRI based on (*i*) presence or absence of a hypercapnia response, (*ii*) comparison of signal change during hypercapnia and visual stimulation, and (*iii*) response timing of the visual FMRI data. Experiment 3 acquires hypercapnia data in three subjects with high b value diffusion weighting applied along two orthogonal directions, with the goal of assessing the directional dependence of the DFMRI signal. All experiments acquired both DFMRI scans and conventional FMRI data, which exhibit T_2^* BOLD contrast. In addition to sensitivity to diffusion, the DFMRI data are also sensitive to T_2 BOLD effects, which are the only source of contrast at $b = 0$ s/mm^2. The basic paradigm for each experiment

Author contributions: K.L.M., D.P.B., R.G.W., M.W.W., P.J., and T.E.J.B. designed research; K.L.M., D.P.B., H.D., and M.D.R. performed research; K.L.M. and T.E.J.B. analyzed data; and K.L.M. and T.E.J.B. wrote the paper.

The authors declare no conflict of interest.

This article is a PNAS Direct Submission.

[‡]To whom correspondence should be addressed. E-mail: karla@fmrib.ox.ac.uk.

This article contains supporting information online at www.pnas.org/cgi/content/full/0707257105/DC1.

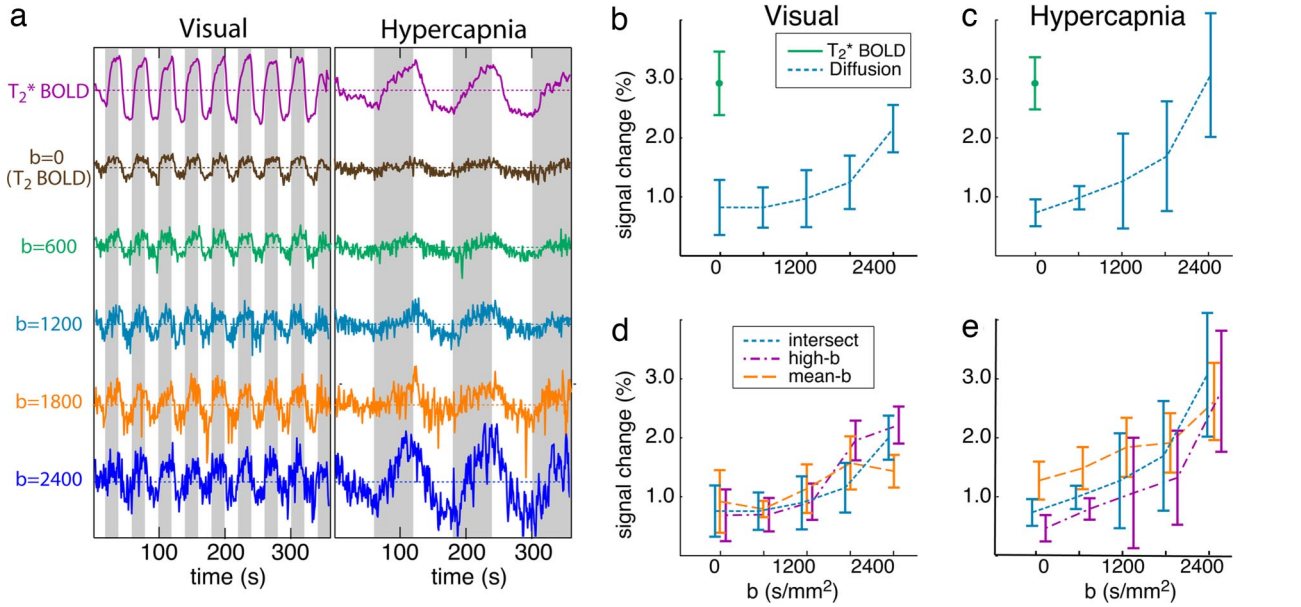

Fig. 1. Results from Experiments 1 (visual) and 2 (hypercapnia) combined across all subjects. (*a*) Mean subject time course within the ''intersect'' ROI for each imaging condition. Gray swathes indicate stimulation periods. All plots are scaled to the same percent signal change. (*b–e*) The percent signal as a function of *b* value, with each condition plotted as intersubject mean ± intersubject standard deviation. (*b* and *c*) The percent signal change in the ''intersect'' ROI, including BOLD (green) and DFMRI (blue), over the range of acquired *b* values. (*d* and *e*) Percent signal change in the DFMRI data for the different ROI selection methods (plots are horizontally staggered to aid in visualization).

is listed in Table 1, and further details, including region-of-interest (ROI) definition, are described in *Methods*.

Comparison of Hypercapnia and Visual Responses. The intersubject mean time courses for Experiments 1 (visual) and 2 (hypercapnia) are shown in Fig. 1*a*. Representative activation maps, which are binarized to generate the ROIs, are given in supporting information (SI) Figs. 4 and 5). All subjects exhibited statistically significant signal changes under all conditions (for both visual and hypercapnia stimuli, and at all *b* values). The $b = 0$ data are known to detect T_2 BOLD, which is closely related to the T_2^*-based contrast used in conventional FMRI. Fig. 1 *b* and *c* demonstrates a statistically significant increase in the percent signal change with increasing *b* value (paired *t* test, $P < 0.01$). This result holds for all ROI selection methods (Fig. 1 *d* and *e*), is similar for visual and hypercapnic stimulation, and consistent with data reported in the visual cortex (figure 2*a* in ref. 18). All subjects exhibited an increase in the percent signal change at high *b* value for both visual and hypercapnia data, and results for each subject are included in SI Figs. 6 and 7). Interestingly, the $b = 2{,}400$ s/mm^2 DFMRI data and T_2^* BOLD data have similar response magnitude for both visual and hypercapnia stimuli (2–3%, shown for the "intersect" ROI in Fig. 1 *b* and *c*), suggesting consistency between the T_2^* BOLD response and the DFMRI data at high *b* value. The existence of a response to hypercapnia at high *b* value, along with the consistency of the DFMRI data for hypercapnia and visual stimuli, is suggestive of a vascular contribution to the signal.

Table 1. Basic paradigm for the three presented experiments

Experiment	Stimulus	*b* values, s/mm^2	Diffusion directions
1	Visual	0–2,400	$x + y$
2	CO_2	0–2,400	$x + y$
3	CO_2	1,800	$x + y$, $x - y$

Timing Characteristics (Visual). Previous work reported an early response at high *b* value compared with low *b* value (18) that was suggested to precede any possible hemodynamic changes. The mean response to a single visual stimulus block (Experiment 1) is plotted in Fig. 2*a* and does not appear to exhibit an earlier response at high *b* value (i.e., a fast response for $b \geq 1{,}800$ s/mm^2 compared with $b = 0$ s/mm^2). The root-mean-squared error (ε, see Eq. **1**) can be used to quantify the onset delay of the T_2^* BOLD data compared with a time-shifted version of the DFMRI data (Fig. 2*b*). An earlier signal onset at high *b* value would be manifested as a negative shift of the minimum in Fig. 2*b*, or a negative shift in the zero crossing of the derivative of this error, shown in Fig. 2*c*. Fig. 2 *d–f* depicts the optimal time-shift for three signal models with different timing parameters (most importantly the assumed response delay, τ) and three ROI selection methods. A slight negative shift ($\approx$0.5 s) is found at all *b* values, which is driven by the difference in shape between the DFMRI time course and the T_2^* BOLD time course. The expected early response would appear as a more negative Δt at high *b* value. There is no such trend in the data for $b = 600$–$1{,}800$ s/mm^2, and only a small effect (0.4–0.7 s) at $b = 2{,}400$ s/mm^2 (which is significant only when the data are analyzed by using $\tau = 2$ s). These results are summarized with significance tests in SI Table 2. The timings included in these analyses capture the full range of expected behavior: from an immediate response with $\tau = 0$ s to the standard hemodynamic delay $\tau = 6$ s. There is no consistent trend for a faster response at high *b* value, and the small shifts that are significant are well within the range of time delays in the vascular bed; no observed shift is in the previously reported range of 2–4 seconds (18). The lack of an early response at high *b* value suggests that the signal reflects slow hemodynamic processes rather than a fast neuronal response.

Directional Dependence (Hypercapnia). The diffusion weighting used here and in previous studies at high *b* value (17, 18) is applied along a single direction, which could cause the signal change to reflect the orientation of the diffusion-sensitized direction relative to local

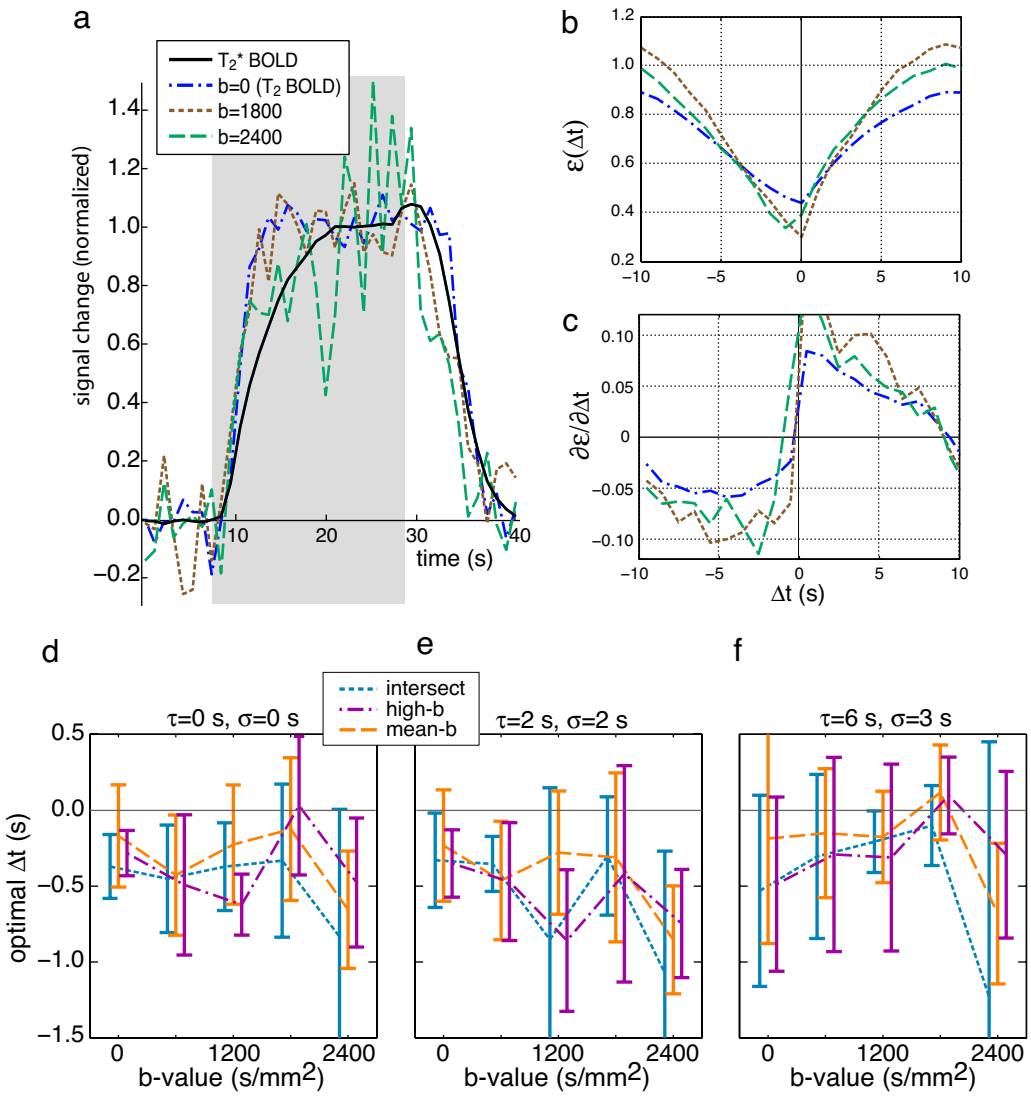

Fig. 2. Timing analysis for the visual experiment. (*a*) Intersubject mean response to a single block of visual stimulation. All time courses are normalized to unit plateau for timing analysis. The stimulus duration is noted by the gray swathe (the time courses have been shifted by 8 seconds for ease of display). (*b*) Normalized RMS error between T_2^* BOLD and time-shifted DFMRI time-courses. This error is minimized when the two curves are maximally aligned, and the shift (Δt) at which this occurs will be referred to as the ''optimal time shift.'' (*c*) Derivative of the normalized RMS error shown in *b*, which will cross zero at the optimal time shift. (*d–f*) The optimal time shift for the different ROI selection methods (''intersect,'' ''mean-b,'' and ''high-b'') and several signal models with slight changes in the expected timing of the signal (where τ delays and σ smoothes the time course). Previous work has reported an optimal time shift at high *b* value that is 2–4 seconds earlier than at low *b* value. No significant difference of this kind is observed in our data.

tissue/vessel microstructure. It has been suggested that a directionally selective response to cell swelling might occur in highly oriented tissues (28), but not for the (roughly spherical) cell bodies of gray matter. In contrast, the vascular network within cortex is highly ordered, with different vessel types and vascular layers running either parallel or perpendicular to the cortical surface (29). It may therefore be informative to investigate the dependence of the DFMRI signal on the direction of weighting, although any results must be considered anecdotal and interpreted with caution. The dependence of the hypercapnia response at high *b* value on the direction of diffusion weighting (Experiment 3) is demonstrated in Fig. 3. All three subjects demonstrated hypercapnia-induced signal changes that had a strong spatial dependence on the direction of diffusion weighting (see Fig. 3 *a–c*). In general, these patterns exhibited right–left symmetry, where a region that activated during $x + y$ weighting was activated on the contralateral side during x–y weighting and vice versa. This response was strongly directional, with a small percentage of the activated voxels (12–17%) responding for both directions. Despite noticeable intersubject variability, these patterns were sufficiently reproducible to be significant in a fixed-effects group analysis (Fig. 3 *d–f*). Comparing the DFMRI signal (red and blue color maps) to the T_2^* BOLD signal (green color map), the combined extent of activation across the two diffusion-weighted directions are similar to the extent of BOLD activation, albeit at lower contrast-to-noise ratio. This observation was confirmed with the appropriate contrast at the group level, but is not shown for brevity. The existence of directional dependence in the DFMRI response at high *b* value is intriguing but should be interpreted cautiously, as discussed below.

Discussion

Several aspects of our data suggest that the DFMRI response at high *b* value has a significant vascular component. First, the existence of a signal response during hypercapnia is consistent

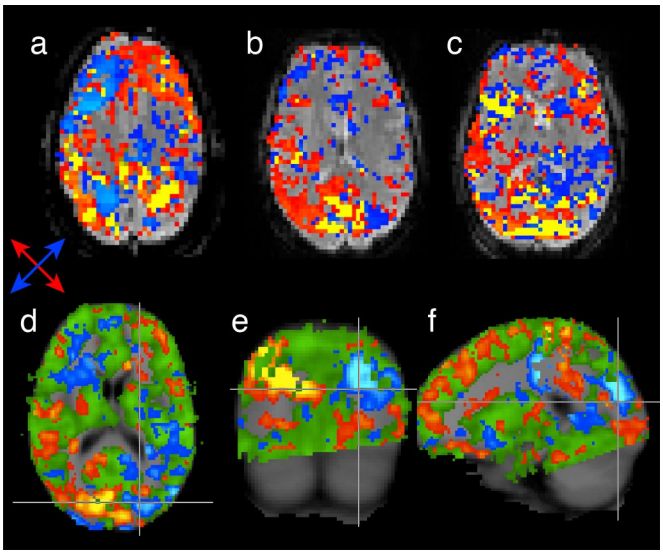

Fig. 3. Activation maps for Experiment 3 demonstrate the dependence of the regions of activation on the direction of diffusion weighting. The images in (*a–c*) show representative slices in the three scanned subjects where the red color map indicates superthreshold parameter estimates during diffusion weighting along the *x–y* direction (see red arrow), blue indicates significance during *x* + *y* weighting (blue arrow) and yellow indicates the overlap (regions active during both conditions). Each subject exhibits a high degree of heterogeneity for the different weighting directions, with strong right–left asymmetry. Only 12–17% of the activated voxels lay in the overlap region (by subject: 12% of 3,681, 16% of 8,335 and 17% of 12,118 voxels). (*d–f*) Group fixed-effects analysis in standard space. The red and blue color-coding is the same as *a–c*, but the green color map is the group fixed-effects map for the BOLD data (which provides a reference for highly perfused regions). The right–left asymmetry is significant at the group level, indicating consistent dependence of the hypercapnia response on the direction of diffusion weighting.

with the blood flow response to increased CO_2, which has little or no effect on neuronal activity. Second, the similarity of the signal dependence on *b* value during hypercapnia and visual stimulation is suggestive of a common signal source, implicated as a vascular effect by the presence of a hypercapnia response. Third, the signal changes in T_2^* BOLD and high *b* value diffusion are approximately matched for these two very different stimulation paradigms, again suggesting a common source. Fourth, a thorough analysis of the timing characteristics of our visual experiment failed to reproduce the previously reported early response in DFMRI at high *b* value.

The interpretation of the hypercapnia data relies on the assumption that no swelling of the brain cells occurs in response to hypercapnia. Although there is some controversy as to whether hypercapnia induces no change in neuronal firing rates (22, 23) or a mild depression in firing rates due to reduced excitability (24, 30, 31), our signal increases would only be consistent with an *increase* in firing rate, which has not been reported. In addition to neuronal activity, it is important to consider other possible sources of hypercapnia-induced cell swelling. In some cell populations, hypercapnia results in the conversion of CO_2 and H_2O to bicarbonate (HCO_3^-) via the action of carbonic anhydrase, resulting in reduced pH (32). In these tissues, the resulting increase in intracellular osmotic pressure can lead to water influx and therefore cell swelling. However, a number of studies have established that brain cells do not swell within the normal, healthy range of pH (7.35–7.45), instead exhibiting an all-or-none swelling of 15–20% once the pH drops below the critical threshold of 6.8 (33–36). This critical threshold applies to both glia (33, 34, 36) and neurons (35), and corresponds to the pH range found in ischemia and trauma (34, 36) and the point at which individuals typically become unresponsive (37). The mild hypercapnia (4% CO_2) used in this study should be well outside the range in which cell swelling occurs.

Although the primary purpose of this article is to report experimental data rather than to propose a precise mechanism for these signal changes, it is nevertheless worthwhile to consider how vascular changes could result in the observed data. One important issue in DFMRI is the amount of intravascular signal that remains at high *b* value. It is frequently assumed in DFMRI that the vascular signal is completely removed when some critical *b* value is exceeded (typically this threshold is considered to be 300–600 s/mm^2). However, several experiments have suggested that residual intravascular signal may exist even at high values (38, 39). The residual vascular signal has been associated with deoxygenated blood in the capillaries or venules (39), which will have a large BOLD effect.

The crucial question, however, is not whether any BOLD signal remains at high *b* value, but rather why the percent signal change rises with increasing *b* value. Le Bihan and colleagues (18, 28) propose that this is caused by two tissue compartments with different diffusion coefficients. During activation, they hypothesize that the compartment with slower diffusion increases (because of cell swelling), causing the overall diffusion to decrease and the signal to therefore increase. However, a similar effect could arise for compartments with fixed volume (no swelling) that had different diffusion coefficients and T_2 values (40). As the *b* value changes, the signal contribution of the T_2 BOLD effect in each compartment would be determined by its diffusion coefficient, and the percent signal change would therefore depend on *b* value. For example, veins and capillaries are possible compartments: these vessels have different T_2 BOLD effects because of their varying oxygenation levels, and would be expected to have different apparent diffusion coefficient based on vessel size. However, a range of possible compartments exist, and the close relation between T_2 and diffusion coefficient make this a compelling possibility.

A related but distinct possibility suggested by our results is that the DFMRI signal at high *b* value depends on the direction of diffusion weighting. Directional diffusion weighting could conceivably attenuate signal from vessels with a component parallel to the direction of weighting while leaving residual signal from vessels perpendicular to the diffusion vector (i.e., vessels with a significant component in the plane that is orthogonal to the weighting). Our data would be consistent with residual, intact signal from vessels with ordered geometry, as occurs in cerebral cortex (29). For our results to be consistent with the cell swelling hypothesis, the swelling would have to be strongly anisotropic, which might be expected in highly structured tissue like white matter (28) but is less likely for the (approximately spherical) cell bodies in gray matter.

Several of these possibilities attribute the residual BOLD signal to capillaries and venules. Such a mechanism could give rise to a slightly earlier signal due by selectively attenuating draining veins, where the oxygenation changes lag by 1–2 seconds because of the delayed transit time. This is a possible source for the small shifts of 0.40–0.75 seconds observed at the highest *b* value. Similar time-shifts in DFMRI have been suggested at low *b* value (15, 16).

Further studies will be required to determine which, if any, of the above possible mechanisms are involved. These explanations all relate to selective nulling of signal components by the diffusion weighting, and therefore can be studied based on the proposed compartmentalization. For example, one could compare directional and isotropic diffusion weighting to determine whether the residual signal is based on vessel geometry. There are also other possible sources, including changes in cerebral blood volume (16) or interactions of the diffusion-weighting gradients with background susceptibility gradients (41, 42).

In conclusion, although it is impossible to rule out a contribution due to cellular swelling, the results presented here are highly suggestive that the DFMRI response at high *b* value has a significant vascular component. If a contribution due to cellular swelling does exist, our results indicate that great care must be taken to avoid the accompanying vascular response to isolate a direct measure of neuronal activity.

Methods

Stimulus. In Experiment 1, seven healthy subjects viewed a blue and yellow annular checkerboard pattern reversing at 8 Hz for 20 seconds, followed by a fixation point for 20 seconds. In each run, nine stimulus blocks were used for a total of six minutes per run. In Experiment 2, the same seven subjects breathed 1-minute blocks of 4% inspired CO_2 in balance air, followed by 1 minute of normal air, cycled three times for a total of 6 minutes per run. This level of hypercapnia provides a mild (minimally noxious) stimulus with a robust change in the BOLD signal. Experiments 1 and 2 acquired data at a range of *b* values along a single direction of diffusion weighting. In Experiment 3, three of the subjects were scanned again with the same hypercapnia paradigm used in Experiment 2, except that six blocks were acquired for a total of 12 minutes per run. Experiment 3 investigates the dependence of the signal on the direction of diffusion weighting, and acquired data at a single *b* value along three different directions. Subjects were all experienced with hypercapnia and tolerated the challenge well. To reduce motion, subjects were comfortably restrained with soft padding at the temples.

Image Acquisition. Imaging used a Siemens 3T Trio scanner (12-channel receive coil, 40 mT/m gradients), with acquisition parameters closely matched to (18). The diffusion acquisition used a doubly refocused spin echo (43) with a single-shot echo-planar-imaging acquisition. The hardware and acquisition software were supplied by the same vendor as that used in the previous study (18) and, to our knowledge, are closely matched. This pulse sequence is diagrammed in SI Fig. 8.

In Experiments 1 and 2, five DFMRI runs were acquired at the same *b* values used in ref. 18 ($b = 0$, 600, 1,200, 1,800, 2,400 s/mm^2) along a single direction in the axial plane ($x + y$ in the scanner frame of reference). The highest *b* value was repeated once to boost the contrast-to-noise ratio. Imaging parameters were optimized to enable a short T_R (for timing analysis in Experiment 1) and T_E (for SNR), which restricted acquisition to seven slices ($T_E = 100$ ms, $T_R = 1$ s, field-of-view = 22 cm, $64 \times 64 \times 7$ matrix, 6/8 partial k-space, 3.4-mm thickness, bandwidth = 1,628 Hz/pix, for interecho spacing 0.69 ms and acquisition window 33 ms). We also acquired one run with T_2^* BOLD contrast using a gradient echo acquisition with identical parameters to the DFMRI runs, but with $T_E = 30$ ms. In Experiment 3, three DFMRI runs were acquired at a single *b* value ($b = 1{,}800$ s/mm^2) along three different directions ($x + y$, $x - y$, z). This experiment used a longer T_R to enable increased coverage with 22 slices, and a shorter T_E was achieved because of the smaller *b* value ($T_E = 95$ ms, $T_R = 3$ s, field-of-view = 22 cm, $64 \times 64 \times 22$ matrix, 6/8 partial k-space, 3.4-mm thickness, bandwidth = 1,628 Hz/pix). A T_2^* BOLD run ($T_E = 30$ ms) was also acquired for reference. Although data were acquired with diffusion weighting along *z*, these data had high temporal variance because of cardiac pulsatility (44) and were discarded.

Time-Series Analysis. The visual data were high-pass filtered (full-width at half-maximum equal to the stimulus period of 40 s) to remove slow trends, and then analyzed with FSL (45) by using rectangular waveforms representing the stimulus periods convolved with a kernel representing the hemodynamic response (a single-gamma characterized by a delay, τ, and temporal blur, σ). Analysis of the visual data were repeated with several different kernels: (*i*) no kernel, to avoid any bias ($\tau = 0$ s, $\sigma = 0$ s, a ''boxcar'' model); (*ii*) a model to match the previously reported diffusion response (18) ($\tau = 2$ s, $\sigma = 2$ s, the ''diffusion response'' model); and (*iii*) the standard hemodynamic kernel ($\tau = 6$ s, $\sigma = 3$ s, the ''hemodynamic response'' model). The hypercapnia data were high-pass filtered (full-width at half-maximum, 120 s), and analyzed with the measured end-tidal CO_2 waveforms filtered to match the hemodynamic response to hypercapnia ($\tau = 5$s, $\sigma = 15$ s). Data were motion-corrected and checked by eye to ensure good alignment, particularly in the high *b* value images. In addition, data at different *b* values were carefully checked for any systematic differences in distortion due to eddy currents, which were found to be minimal because of the doubly refocused diffusion acquisition (43). After standard FMRI analysis, all runs were aligned and several further analyses were performed.

Region-of-Interest (ROI) Definition. For Experiments 1 and 2, ROIs were defined, from which the signal was extracted for further analysis. Several alternative ROIs were generated by thresholding the statistical maps in various ways: (*i*) the ''high-*b*'' ROI was defined by thresholding a fixed-effects map combining the data with $b \geq 1{,}800$ s/mm^2 ($z_{HIGH} \geq 3.0$), (*ii*) the ''mean-b'' ROI was defined by thresholding a fixed-effects map combining the DFMRI data across all *b* values ($z_{MEAN} \geq 3.0$), and (*iii*) the ''intersect'' ROI was defined by taking the intersection of the ''high-*b*'' ROI with a thresholded BOLD activation map ($z_{BOLD} \geq 8.0$). The size of the ROIs used in this study are given in SI Table 3. The average signal time course within each ROI was calculated, and averaged over all subjects to create a single average time course at each *b* value. The percent signal change in a given voxel was calculated as the parameter estimate (fitted effect size) divided by the mean time course signal. This percent signal change was also averaged over the ROI and across subjects to create a mean percent signal change at each *b* value.

Timing Characterization. For Experiment 1 (visual), the timing analysis proposed in ref. 18 was reproduced by using the time course to a single block of visual stimulation at the various *b* values. The normalized root-mean-squared error (ε) between the T_2^* BOLD time course and a time-shifted version of a DFMRI time course was calculated as follows:

$$\varepsilon(\Delta t) = \sqrt{\frac{\sum_t (S_{\mathrm{BOLD}}(t) - S_{\mathrm{DFMRI}}(t - \Delta t))^2}{\sum_t S_{\mathrm{BOLD}}(t)^2}}. \qquad [1]$$

This function is minimized at the temporal delay, Δt, at which the BOLD and diffusion time courses are maximally correlated. This minimum can be more easily quantified as the Δt at which $\delta\varepsilon/\delta\Delta t = 0$. To isolate the effects of the signal onset, this analysis only included the 10 seconds before and after stimulus onset (i.e., $t = 10$–30 s in each 40-s block). This reduces artificial shifts that can occur because of differences in the overall shape, which can cause ε to be minimized despite clear mismatch of the signal onset. This analysis was not performed on the hypercapnia data because of the slow signal changes, which makes timing calculations unreliable. Optimal time shifts were calculated for each subject separately, as well as from group average time courses. Cross-subject paired *t* tests were calculated to compare the time shift at $b = 0$ s/mm^2 to the time shift at $b \geq 0$.

Spatial Characterization. The dependence of the diffusion response on the direction of diffusion weighting was investigated in Experiment 3. After basic analysis of each diffusion direction (as described above), each subject was aligned to the MNI152 standard space for several group-level analyses. The dependence on diffusion weighting was calculated in a two-stage analysis: the first stage (performed separately on each subject) modeled the brain regions that preferentially activated in the $x + y$ condition compared with the $x - y$ condition; the second stage consisted of a fixed effects analysis to combine the subjects in standard space. The output of this analysis was a statistical map that was thresholded to indicate regions for which $x + y > x - y$ ($z \geq 2.0$) and regions for which $x + y < x - y$ ($z \leq -2.0$). A second group-level analysis was performed to determine the regions of the brain that were activated in the BOLD data (fixed effects across all subjects, maps thresholded at $z \geq 5.0$). This analysis serves as a useful reference for brain regions that have a known blood flow response to hypercapnia.

ACKNOWLEDGMENTS. We thank Denis Le Bihan for insightful discussions and comments on the manuscript. K.L.M. was funded by the Royal Academy of Engineering/Engineering and Physical Sciences Research Council Research Fellowship.

1. Fox PT, Mintun MA, Raichle ME, Miezin FM, Allman JM, van Essen DC (1986) *Nature* 323:806–809.
2. Posner MI, Peterson SE, Fox PT, Raichle ME (1988) *Science* 240:1627–1631.
3. Ogawa S, Tank DW, Menon R, Ellermann JM, Kim S-G, Merkle H, Ugurbil K (1992) *Proc Natl Acad Sci* 89:5951–5955.
4. Kwong KK, Belliveau JW, Chesler DA, Goldberg IE, Weisskoff RM, Poncelet BP, Kennedy DN, Hoppel BE, Cohen MS, Turner R, *et al.* (1992) *Proc Natl Acad Sci* 89:5675–5679.
5. Kim SG, Richter W, Ugurbil K (1997) *Magn Reson Med* 37:631–636.
6. Turner R (2002) *NeuroImage* 16:1062–1067.
7. Boynton GM, Engel SA, Glover GH, Heeger DJ (1996) *J Neurosci* 16:4207–4221.
8. Logothetis NK, Paus J, Augath M, Trinath T, Oeltermann A (2001) *Neuron* 412:150–157.
9. Fox PT, Raichle ME (1986) *Proc Natl Acad Sci* 83:1140–1144.
10. Davis TL, Kwong KK, Weisskoff RM, Rosen BR (1998) *Proc Natl Acad Sci* 95:1834–1839.
11. LeBihan D (1988) *Magn Reson Med* 7:346–351.

12. LeBihan D, Turner R, Macfall JR (1989) *Magn Reson Med* 10:324–337.
13. LeBihan D, Turner R (1991) *Magn Reson Med* 19:221–227.
14. Song AW, Wong EC, Tan SG, Hyde JS (1996) *Magn Reson Med* 35:155–158.
15. Gangstead SL, Song AW (2002) *Magn Reson Med* 48:385–388.
16. Harshbarger TB, Song AW (2004) *Magn Reson Med* 52:1432–1437.
17. Darquie A, Poline JB, Poupon C, Saint-James H, Bihan DL (2001) *Proc Natl Acad Sci* 98:9391–9395.
18. LeBihan D, Urayama S, Aso T, Hanakawa T, Fukuyama H (2006) *Proc Natl Acad Sci* 103:8263–8268.
19. Turner R, LeBihan D, Maier J, Vavrek R, Hedges LK, Pekar J (1990) *Radiology* 177:407–414.
20. Michelich CR, Song AW, MacFall JR (2006) *NMR Biomed* 19:566–572.
21. Hoge RD, Atkinson J, Gill B, Crelier GR, Marrett S, Pike GB (1999) *Proc Natl Acad Sci* 96:9403–9408.
22. Krnjević K, Randić J, Siesjö BK (1965) *J Physiol* 176:105–122.
23. Jones M, Berwick J, Hewson-Stoate N, Gias C, Mayhew J (2005) *NeuroImage* 27:609–623.
24. Martin C, Jones M, Martindale J, Mayhew J (2006) *Eur J Neurosci* 24:2601–2610.
25. Kety SS, Schmidt CF (1948) *J Clin Invest* 27:484–492.
26. Horvath I, Sandor NT, Ruttner Z, McLaughlin AC (1994) *J Cereb Blood Flow Metabol* 14:503–509.
27. Yang SP, Krasney J (1995) *J Cereb Blood Flow Metabol* 15:115–123.
28. LeBihan D (2007) *Phys Med Biol* 52:57–90.
29. de la Torre FR, Rodriguez-Baeza A, Sahuquillo-Barris J (1998) *The Anatomical Record* 251:87–96.
30. Aram JA, Lodge D (1987) *Neurosci Lett* 83:345–360.
31. Balestrino M, Somjen GG (1988) *J Physiol* 396:247–266.
32. Chesler M (2003) *Physiol Rev* 83:1183–1221.
33. Kempski O, Staub F, Jansen M, Schodel F, Baethmann A (1988) *Stroke* 19:385–392.
34. Staub F, Baethmann A, Peters J, Weigt H, Kempski O (1990) *J Cereb Blood Flow Metabol* 10:866–876.
35. Staub F, Mackert B, Kempski O, Peter J, Baethmann A (1993) *J Neurol Sci* 119:79–84.
36. Plesnila N, Haberstok J, Peters J, Kolbl I, Baethmann A, Staub F (1999) *J NeuroTrauma* 16:831–841.
37. Martini R (1998) *Fundamentals of Anatomy and Physiology.* (Prentice Hall), 6th Ed.
38. Neil JJ, Ackerman JJH (1992) *J Magn Reson* 97:194–201.
39. Duong TQ, Kim S-G (2000) *Magn Reson Med* 43:393–402.
40. Kershaw J, Tomiyasu M, Kashikura K, Hirano Y, Nonaka H, Hirano M, Ikehira H, Kanno I, Obata T (2007) *Proc Int Soc Magn Res Med* p. 25.
41. Zhong J, Kennan RP, Gore JC (1991) *J Magn Reson* 95:267–280.
42. Karlicek RF, Lowe IJ (1980) *J Magn Reson* 37:75–91.
43. Reese TG, Heid O, Weisskoff RM, Wedeen VJ (2003) *Magn Reson Med* 49:177–182.
44. Jiang H, Golay X, van Zijl PCM, Mori S (2002) *Magn Reson Med* 47:818–822.
45. Smith SM, Jenkinson M, Woolrich MW, Beckmann CF, Behrens TEJ, Johansen-Berg H, Bannister PR, Luca MD, Drobnjak I, Flitney DE, *et al.* (2004) *NeuroImage* 23:S208–S219.